Scalable Fabrication of Polymer Membranes with Vertically Aligned 1 nm Pores by Magnetic Field Directed Self-Assembly

Xunda Feng,[†] Marissa E. Tousley,[†] Matthew G. Cowan,[‡,§] Brian R. Wiesenauer,[‡] Siamak Nejati,[†] Youngwoo Choo,[†] Richard D. Noble,[§] Menachem Elimelech,[†] Douglas L. Gin,[‡,§] and Chinedum O. Osuji*[,†]

[†]Department of Chemical and Environmental Engineering, Yale University, New Haven, Connecticut 06511, United States, [‡]Department of Chemistry and Biochemistry, University of Colorado, Boulder, Colorado 80309, United States, and [§]Department of Chemical and Biological Engineering, University of Colorado, Boulder, Colorado 80309, United States

ABSTRACT There is long-standing interest in developing membranes possessing uniform pores with dimensions in the range of 1 nm and physical continuity in the macroscopic transport direction to meet the needs of challenging small molecule and ionic separations. Here we report facile, scalabe fabrication of polymer membranes with vertically (*i.e.*, along the through-plane direction) aligned 1 nm pores by magnetic-field alignment and subsequent cross-linking of a liquid crystalline mesophase. We utilize a wedge-shaped amphiphilic species as the building block of a thermotropic columnar mesophase with 1 nm ionic nanochannels, and leverage the magnetic anisotropy of the amphiphile to control the alignment of these pores with a magnetic field. *In situ* X-ray scattering and subsequent optical microscopy reveal the formation of highly ordered nanostructured mesophases and cross-linked polymer films with orientational order parameters of *ca*. 0.95. High-resolution transmission electron microscopy (TEM) imaging provides direct visualization of long-range persistence of vertically aligned, hexagonally packed nanopores in unprecedented detail, demonstrating high-fidelity retention of structure and alignment after photo-cross-linking. Ionic conductivity measurements on the aligned membranes show a remarkable 85-fold enhancement of conductivity over nonaligned samples. These results provide a path to achieving the large area control of morphology and related enhancement of properties required for high-performance membranes and other applications.

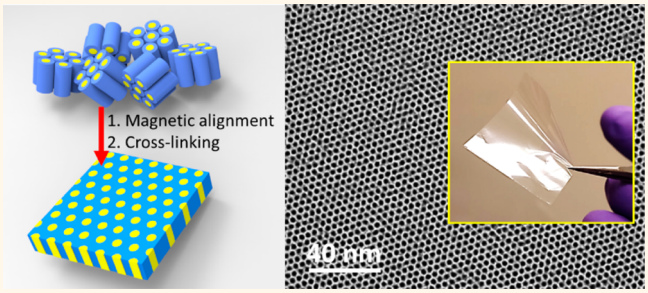

KEYWORDS: directed self-assembly · nanoporous polymers · aligned membranes · magnetic alignment · LC mesophase · ionic conductivity

The ability to precisely and reliably control morphology over large length scales is essential for exploiting many of the functional properties of self-assembled soft materials. This capability is critical in a variety of applications including, for example, photonic band gap materials where uniform optical properties are desired over macroscopic length scales (>1 mm).[1] It is also the case in nanostructured, porous polymer membranes where uniform alignment of the pores parallel to the macroscopic transport direction is required to optimize membrane transport properties.[2,3] However, polymer membranes produced by conventional fabrication techniques (*e.g.*, phase inversion precipitation) possess kinetically controlled pores of random size and orientation, which limits membrane permeability and selectivity. Self-assembled materials exhibit domains with characteristic length scales that are thermodynamically defined. As a result, such materials have the potential to break the long-standing selectivity-permeability trade-off that is intrinsic to the kinetically controlled microstructures of many state-of-the-art membranes.[4,5]

Block copolymer (BCP) nanostructures and small-molecule liquid crystal (LC) mesophases represent two attractive platforms for designing nanoporous polymer membranes with well-defined structures.

* Address correspondence to chinedum.osuji@yale.edu.

Received for review September 6, 2014 and accepted October 26, 2014.

Published online October 26, 2014
10.1021/nn505037b

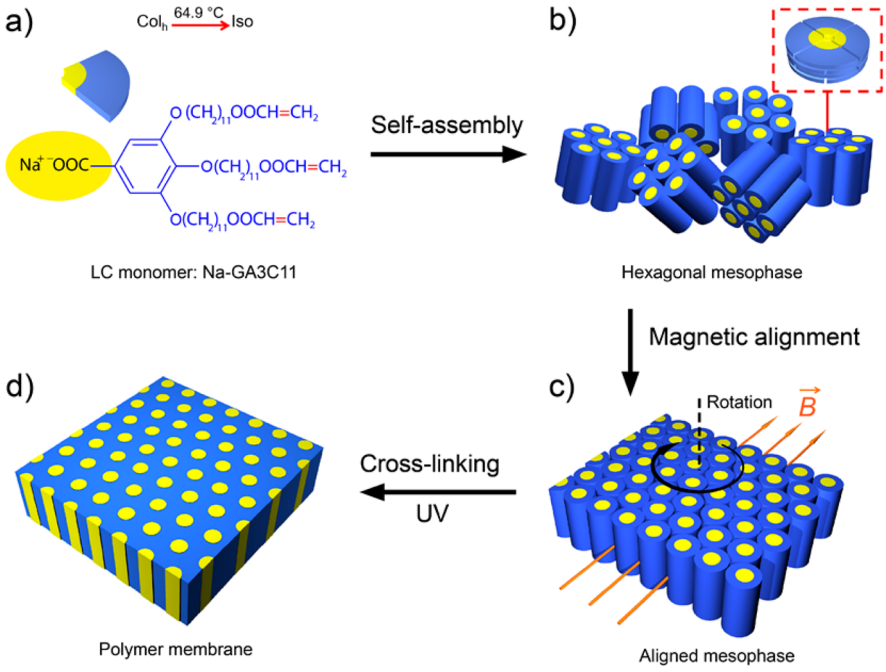

Figure 1. (a) Molecular structure and model of Na-GA3C11 consisting of a small hydrophilic head (yellow) and a large hydrophobic body (blue) with polymerizable acrylate tails. The system transitions from the Col$_h$ to isotropic phase at 64.9 °C as indicated. (b) Thermotropic Col$_h$ mesophase formed by packing neat Na-GA3C11 into disks and stacking the disks into close-packed columns. An inner ionic channel, the *ca.* 1 nm pore, is located at the center of each column. (c) Magnetic-field-driven nondegenerate alignment of the Col$_h$ mesophase by sample rotation about an axis (black line) perpendicular to the field (orange lines). (d) Photo-cross-linking of the aligned Col$_h$ mesophase resulting in a mechanically robust polymer membrane with vertically oriented cylindrical nanopores.

Microphase-separated BCPs have been successfully engineered into functional membranes for ultrafiltration,[6] fuel cells,[7] and rechargeable batteries,[8] with the characteristic pore dimensions controlled by the molecular weight of the polymer. The inverse relationship between molecular weight and the Flory interaction parameter required for self-assembly places a lower bound of *ca.* 5 nm on the pore diameter that can be realized through typical BCP self-assembly.[9,10] As a practical matter, BCP membranes are not ideally suited to address compelling applications in which efficient size-based exclusion of small (<5 nm) organic solutes and ionic species represent pressing needs, notably, in water purification.[11]

By contrast, thermotropic and lyotropic LC mesophases formed by amphiphilic small molecules possess significantly smaller characteristic dimensions than BCPs and offer access to $\leq$1 nm pore sizes.[12] This opens up the possibility of performing highly selective small molecule and gas separations, as well as water desalination based on molecular size-exclusion of hydrated salt ions.[13−16] A useful strategy here has been to utilize polymerizable LC species. The fluidity of the LC enables formation of highly ordered nanostructured porous phases that can then be cross-linked to provide a mechanically robust system. Materials derived in this manner have been applied toward catalysis,[17] adsorption,[18] and ion transport.[19−21] However, preservation of the LC structure during cross-linking can be a challenging proposition, due to reaction (polymerization)-induced phase separation.[22] This issue has arisen in polymerization of many lyotropic LC systems, where the growing polymer chains phase-separated from the lyotropic LC template, resulting in polymers with complete loss of the LC order or less order than the LC template. Moreover, the vertical (through-plane) alignment of transport domains over large areas in thin films required to optimize membrane performance represents a nontrivial challenge.[23] As a result of these challenges, the pursuit of high-performance membrane materials with vertically aligned 1 nm-scale pores based on polymerizable LC mesophases has been significantly hampered to date.

Here, we report the results of efforts designed to effectively circumvent these critical challenges (Figure 1). We use a wedge-shaped amphiphilic monomer (Na-GA3C11) as the building block for forming thermotropic and lyotropic LC mesophases with densely packed (exceeding 10^{12} cm^{-2}), monodisperse cylindrical pores with diameters of *ca.* 1 nm. Physical continuity of the thermotropic LC domains is driven by strong $\pi-\pi$ stacking interactions, and structural locking-in of the LC order during cross-linking is targeted by the use of multiple reactive groups per monomer. An external magnetic field is used to direct the self-assembly of the system, resulting in uniform alignment of the nanopores over arbitrary length scales in arbitrary orientations as dictated by the geometry of the

field relative to the sample. Further, we demonstrate high fidelity retention of the mesophase structure upon cross-linking. The resulting material is a mechanically robust, transparent polymer film. High-resolution transmission electron microscopy (TEM) imaging shows that the pores exhibit physical continuity over strikingly large distances and that vertical pore alignment persists to the exterior surfaces of the film. Ion-transport studies show a remarkable 85-fold increase in the conductivity of the aligned membranes derived from the thermotropic columnar hexagonal phase (Col_h) relative to nonaligned materials with randomly oriented nanopores. Additionally, we show that these magnetic field alignment techniques can be successfully applied to the lyotropic inverted hexagonal (H_{II}) phase (with water-filled ionic nanochannels) formed by the same monomer in the presence of water and an organic comonomer.

RESULTS AND DISCUSSION

The molecular structure of the amphiphilic LC monomer, Na-GA3C11, is shown in Figure 1a. The synthesis is described in Supporting Information. This type of wedge- or fan-shaped amphiphilic species possesses a small hydrophilic, ionic head and a large hydrophobic body, and exhibits both thermotropic and lyotropic LC phases with hexagonal morphologies.[24−27] In its neat state, Na-GA3C11 self-assembles into a thermotropic Col_h phase, or it forms a lyotropic H_{II} phase in the presence of appropriate amounts of water and oil. Here we refer to the Na-GA3C11 itself as the mesogen since it gives rise to the mesophases. In the Col_h phase, this type of mesogen is reported to pack into supramolecular disks consisting of 4 monomers, based on the structure of a sulfonated analogue with similar unit cell dimensions (*d*-spacing of 3.4 nm).[28] These disks then stack to form columns with hexagonal close-packing, resulting in the Col_h mesophase (see Figure 1b). The presence of the Col_h mesophase at room temperature for Na-GA3C11 was confirmed by its birefringent texture in polarized optical microscopy (POM) and the characteristic peak spacing ratio of $1:\sqrt{3}:\sqrt{4}$ from small-angle X-ray scattering (SAXS) (see Supporting Information Figures S2 and S3). The clearing point of the Col_h (T_{iso}) is 64.9 °C, as determined by differential scanning calorimetry (DSC) (see Supporting Information Figure S4). Na-GA3C11 forms similar hexagonally arrayed columnar structures in the lyotropic H_{II} phase but with *ca.* 6 units forming the disks and water-filled ionic channels at the disk center.[29] As elucidated by electron density mapping, this phase has a ~0.9 nm-diameter aqueous pore, with a tunable pore size based on the identity of the metal counterion on the carboxylate group.[30] A pore size estimate of 1.2 nm for the cross-linked H_{II} phase from molecular sieving experiments was consistent with these values.[31]

Magnetic-field alignment of aggregate structures found in LC phases is possible due to the additive effects of the anisotropy in the magnetic susceptibility of individual mesogens, which is sufficient to overcome the disordering effects of Brownian motion.[32−34] Individual uniaxial mesogens possess anisotropy in the diamagnetic susceptibility, χ characterized by $\Delta\chi = \chi_{\parallel} - \chi_{\perp}$, the difference of χ between two orthogonal molecular axes. Individual molecular species typically cannot be aligned by magnetic fields, even at elevated fields, as the reduction in magnetostatic free energy on alignment, $\Delta\chi B^2$, is swamped by thermal energy, kT, and thus, the thermal motion disorders the alignment. Instead alignment results from the collective contributions of individual molecules when ordered thermodynamically into a mesophase, such that the product of the magnetostatic free energy density and the volume of a grain or domain of coherently assembled molecules, $N\Delta\chi B^2$, becomes larger than kT. In the present case, we expect that Na-GA3C11 has an overall positive magnetic anisotropy and that it should align with the field parallel to its long axis, *i.e.*, with the field contained in the plane of the aromatic core. The column axes are perpendicular to the amphiphiles and should therefore align perpendicular to the field (see Figure 1c). This would represent a degenerate scenario as azimuthal distributions of the columns around the field direction would be isoenergetic; the column long axis could lie at any angle in the plane perpendicular to the field direction. This degeneracy can be effectively broken, however, by appropriate rotation of the sample about a vector orthogonal to the field such that the "hard axis" of the system, the columnar long axis, aligns parallel to the axis of rotation (see Figure 1c).[35,36] From a magnetohydrodynamic perspective, the alignment is achieved by imposition of a rotation rate that is faster than the response time of the system defined by the balance of viscous and magnetic torques.[37]

In situ SAXS studies were conducted using a customized SAXS instrument coupled to a magnet (Figure 2a). In this setup, the sample can be rotated about an axis perpendicular to the magnetic field. The orthogonal *x*, *y*, *z* coordinates shown in Figure 2a represent the directions of the rotation axis, the X-ray beam and the magnetic field, respectively. Because of the limited *q*-range of the customized SAXS instrument, only the primary scattering peak of the thermotropic Col_h phase formed by neat Na-GA3C11 at $q^* = 0.176$ Å^{-1} was observable. Alignment was performed by heating a sample above its clearing point and allowing it to cool slowly across the ordering transition in the presence of the field. Figure 2b shows the 2-D SAXS pattern of the statically held sample after slowly cooling (0.1 °C/min) from the isotropic to the Col_h phase at room temperature in a 6 T magnetic field. Anisotropic scattering with intensity concentrated at the top and the bottom of

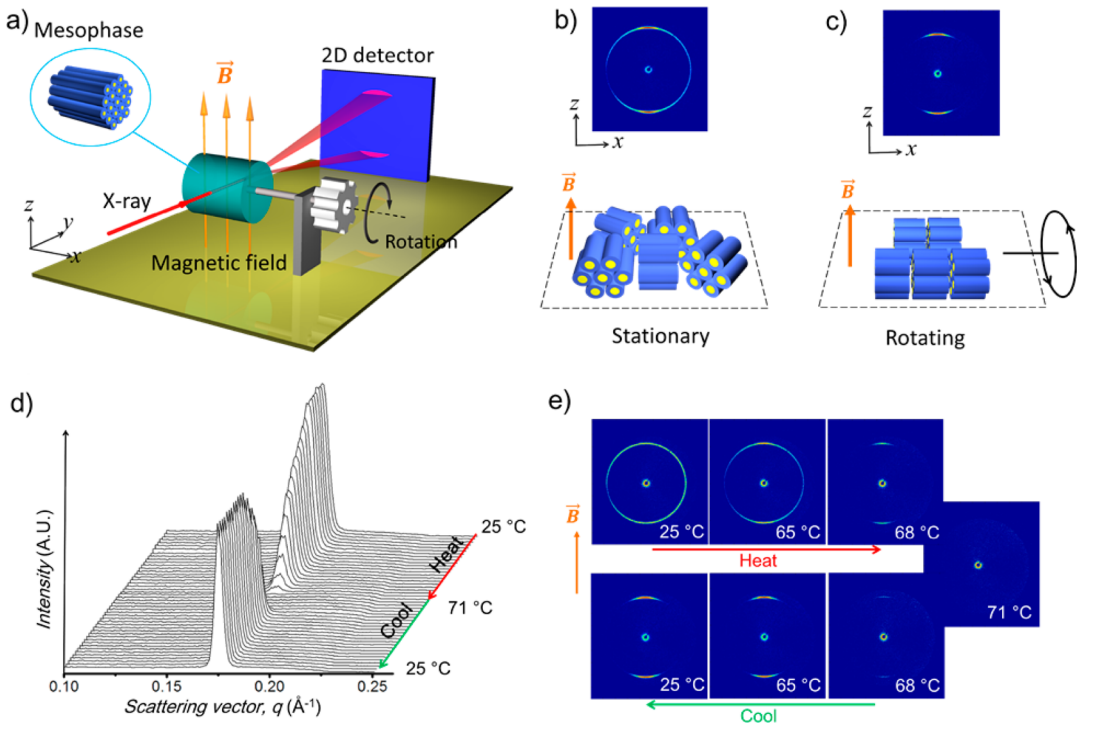

Figure 2. (a) Schematic illustration of the *in situ* SAXS field-alignment experiment. The sample is rotated about an axis (*x*) perpendicular to the magnetic field (*z*-axis) with X-rays incident along the mutually orthogonal *y*-axis. (b, c) Room-temperature 2-D SAXS patterns and 3-D models showing the degenerate alignment of the stationary sample and the unique alignment of the rotated sample, respectively. The diffraction ring corresponds to $q = 0.176$ Å^{-1}, a *d*-spacing of 3.6 nm. (d) Temperature-dependent integrated SAXS data. (e) 2-D patterns of the rotated sample during a heating/cooling cycle in a 6 T magnetic field.

the 2-D diffractogram indicates that the mesophase was aligned by the field. The pattern originates from domains of the supramolecular columns oriented along the *x* axis. However, the pattern also shows detectable scattering at other locations around the primary ring, signifying degenerate orientation of the self-assembled columns in a plane perpendicular to the magnetic field with the column long axes at arbitrary azimuthal angles (Figure 2b). When the sample was simultaneously rotated at 4 rpm about an axis perpendicular to the field while cooling from the isotropic phase, the degeneracy was broken, as evidenced by the two sharp reflections in the 2-D SAXS data. These sharp reflections indicate uniform column alignment along the rotation axis (Figure 2c) and are in good agreement with the expectation that the columns possess a negative diamagnetic anisotropy.

Temperature-resolved SAXS data showing the evolution of the alignment were collected during a heating/cooling cycle (0.1 °C/min) with simultaneous rotation (4 rpm) in the 6 T magnetic field. At 25 °C before alignment, the scattering at $q = 0.176$ Å^{-1} shown in the 1-D integrated data corresponds to the primary Bragg peak of the mesophase (Figure 2d). As the temperature was increased to the isotropic region, the scattering intensity decreased and eventually disappeared at 69 °C. The 2-D diffractograms at different temperatures indicate that the mesophase began to align during the heating process at temperatures in the vicinity of the clearing point (Figure 2e). Upon cooling, the anisotropic scattering pattern reappeared once the temperature was lowered into the LC phase, implying that the hexagonally packed columns form an aligned orientation to the magnetic field. The scattering intensity increased upon cooling the sample back to 25 °C.

Na-GA3C11 with a small amount (0.5 wt %) of photoinitiator was aligned by the 6 T field using the same sample rotation and slow cooling protocol. After alignment, the mesophase was immediately photo-cross-linked by exposure to 365 nm UV light at room temperature. TEM was used to visualize the resulting highly ordered nanostructured polymer. Thin specimens (*ca.* 60 nm thick) were prepared by microtoming either along or perpendicular to the sample rotation axis. The specimens were treated with RuO_4 to provide imaging contrast by selectively staining the benzene rings lining the nanopores.

Figure 3a shows a TEM image of a specimen sectioned perpendicular to the rotation axis. A single-crystal-like hexagonal array of the ionic nanochannels (dark areas), with a *d*-spacing of 3.3 nm, is observed. This TEM image is in good agreement with SAXS, which suggests a *d*-spacing of 3.5 nm. On the basis of these dimensions, the areal pore density is $\sim 2.5 \times 10^{12}$ cm^{-2}, about an order of magnitude higher than that typically

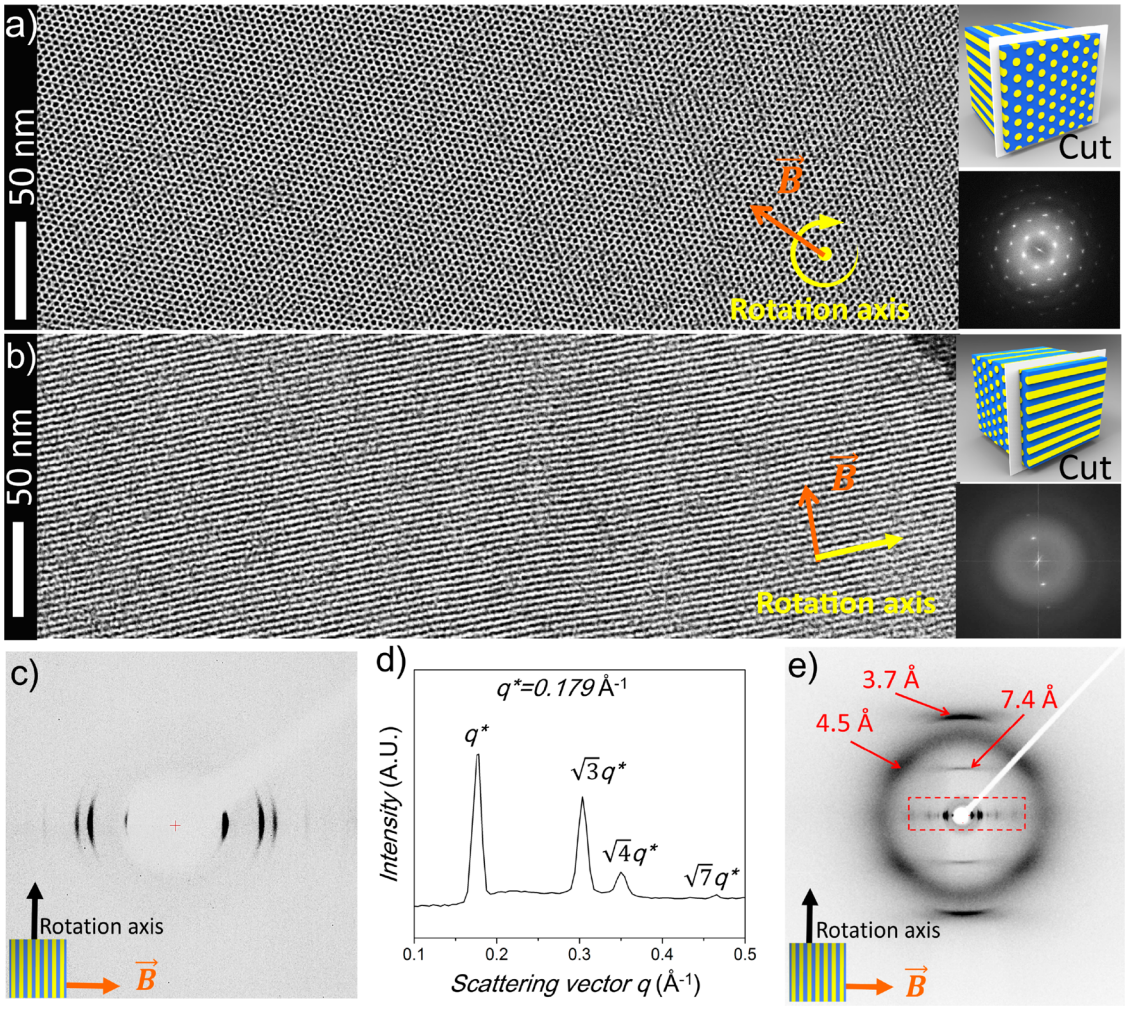

Figure 3. TEM and SAXS data demonstrating large-area, highly ordered hexagonal nanostructures of the cross-linked Col_h phase of Na-GA3C11. The TEM images were obtained by visualizing *ca.* 60 nm thick specimens microtomed (a) perpendicular or (b) parallel to the rotation axis, as schematically illustrated by the insets. Fourier transforms (insets) show 6- and 2-fold symmetry with higher-order contributions, reflecting the high degree of order in the sample. Room-temperature 2-D SAXS pattern (c) and corresponding integrated data (d) of the bulk sample confirm the retention of the aligned structure after polymerization. The primary reflection peak, $q^* = 0.179$ Å^{-1}, corresponds to a *d*-spacing of 3.5 nm. (e) 2-D WAXS pattern of the polymer. The equatorial reflections (dashed rectangle) are due to the vertically aligned columnar structure. The sharp meridional reflections at 3.7 Å correspond to the $\pi-\pi$ stacking along the column and the weaker ones at twice this spacing (7.4 Å) are attributed to longer distance correlations due to 2_1 helical ordering of units around the columnar axis. The 4-fold spots at 4.5 Å are attributed to tilted packing of the alkyl chains.

found in block copolymer derived membranes. The Fourier-transform pattern exhibits sharp 6-fold symmetric contributions, up to four orders, which reflects the high degree of alignment and structural order of the nanochannels. TEM of a sample sectioned along the rotation axis (Figure 3b) provides the complementary view of nanochannels parallel to the axis of rotation, with the Fourier-transform image showing the associated 2-fold symmetry. TEM imaging at lower magnification (Supporting Information Figures S5 and S6) captures the large grain size of the system, with typical correlation lengths of roughly 5 and 1 μm in the along and perpendicular to the columnar axes, respectively. This finding is significant for fabrication of membranes, which require domain continuity over micron length scales along the transport direction (*i.e.*, the membrane film thickness). Our results provide the first direct visualization of uniformly aligned, hexagonally packed 1 nm ionic channels with successful retention of structure and alignment after photo-cross-linking.

For comparison, we also characterized polymer samples obtained by annealing without rotation in the 6 T magnetic field as well as those without magnetic alignment. The degenerate alignment of the static sample was clearly demonstrated by the TEM image showing domains of columns with their long axes pointing along arbitrary directions in the plane perpendicular to the magnetic field (Supporting Information Figure S7). Conversely, the TEM image of the nonaligned sample was characterized by the coexistence of hexagonal and stripe-like patterns (Supporting Information Figure S8).

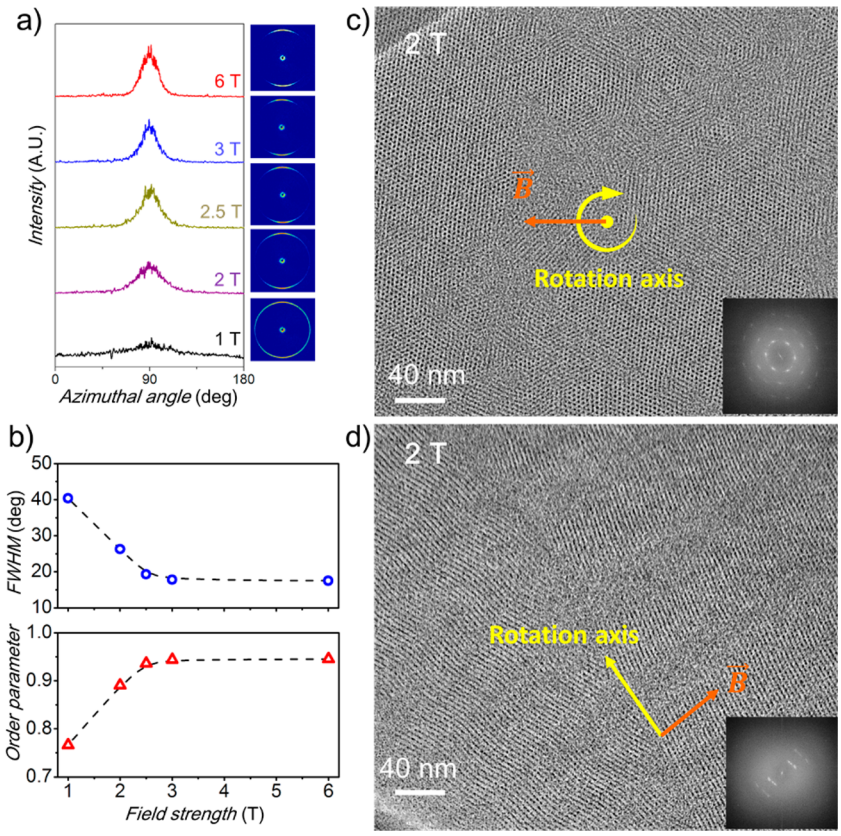

Figure 4. Influence of magnetic field strength on alignment during rotation for the Col_h phase of Na-GA3C11. (a) 2-D SAXS and azimuthal dependence of scattering intensity for different field strengths. (b) Full width at half-maximum (fwhm) and orientational order parameter as a function of field strength. (c, d) TEM images of nanostructured polymers obtained by alignment of the Col_h phase in a 2 T magnetic field viewed perpendicular (c) and parallel to (d) the rotation axis, with Fourier transforms (inset).

Room-temperature SAXS studies also demonstrated the preservation of the highly aligned morphology in the bulk polymer sample. The anisotropic 2-D SAXS pattern (Figure 3c) and the 1-D integrated data with characteristic peak spacing ratio of $1:\sqrt{3}:\sqrt{4}:\sqrt{7}$ (Figure 3d) confirmed the retention of the macroscopically uniform alignment of the hexagonal morphology in the bulk polymer sample. The primary scattering vector q^* shifts from 0.176 (before cross-linking) to 0.179 $Å^{-1}$ (after cross-linking), corresponding to a small shift of the *d*-spacing from 3.6 to 3.5 nm, consistent with a slight shrinkage of the structure after network formation as observed previously for this monomer system.[26,31] The *d*-spacing obtained by SAXS, 3.5 nm, agrees well with that obtained by TEM, 3.3 nm.

Wide-angle X-ray scattering (WAXS) measurements were performed on the aligned cross-linked mesophase to provide insight regarding the intracolumnar assembly relative to the magnetic field (Figure 3e). A series of equatorial reflections are present in the low *q* region (the dashed rectangle), consistent with the orientation of hexagonally packed columns along the rotation axis, as discussed above. The sharp meridional reflections at a Bragg distance of 3.7 Å correspond to the $\pi-\pi$ stacking of the benzene rings between two neighboring discotic superstructures along the columns. This observation implies that the benzene rings are aligned parallel to the magnetic field and is consistent with their known positive diamagnetic anisotropy. The weaker reflections at 7.4 Å, twice the $\pi-\pi$ stacking distance and therefore indicating correlation of every second disc along the columns, are attributed to helical ordering of the mesogens along the columns. The 4-fold spots at 4.5 Å likely originate from tilted packing of the hydrophobic chains. Columnar LC phases formed by many discotic mesogens exhibit similar assembly.[38,39]

The influence of magnetic field strength on the alignment quality of the mesophase was investigated. Figure 4a shows the azimuthal intensity distribution and the 2-D diffractograms for the primary Bragg peak at different field strengths. At a relatively low field strength of 3 T, the mesophase was still able to maintain the well-ordered hexagonal morphology compared to that at 6 T, as evidenced by almost identical full-widths at half-maximum (fwhm) for the Bragg peaks of 17.5° and 17.8°, respectively, shown in Figure 4b. Using a Gaussian approximation for the azimuthal intensity distribution,[40] an orientational order parameter of S_{6T} = 0.95 and S_{3T} = 0.94 can be correlated with these fwhms, where $S = 1$ corresponds to a perfectly oriented system and $S = 0$ to a completely

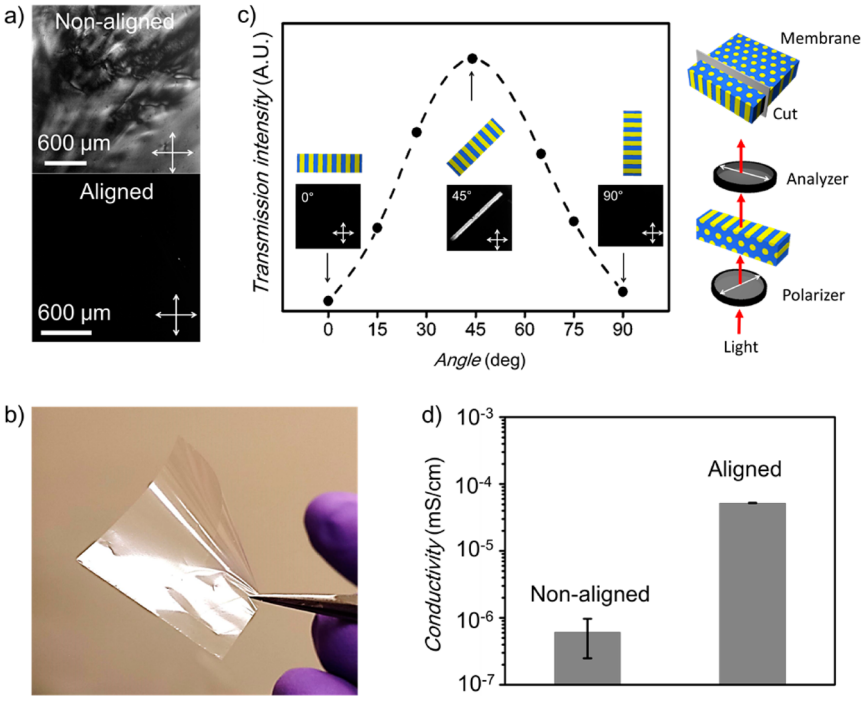

Figure 5. (a) POM images of membranes of the cross-linked Col_h phase of Na-GA3C11 with nonaligned and aligned ionic nanochannels. (b) Photograph of a free-standing cross-linked Col_h membrane of Na-GA3C11 with vertically aligned pores. (c) Transmission intensity of a slice from the aligned membrane under crossed polarized light. The membrane normal is orthogonal to the direction of light propagation. The transmission intensity varies with a 90-degree period, which is consistent with vertically aligned pores. (d) Ionic conductivity of cross-linked Col_h membranes of Na-GA3C11 with nonaligned and aligned pores measured at a relative humidity of 100%. The aligned membranes show an 85-fold enhancement of conductivity over nonaligned samples.

random one. The high-order parameters indicate that the magnetic field aligns the mesophase very effectively. The alignment quality decreased upon reducing the field strength below 3 T, as characterized by an increase of the fwhm and a corresponding decrease of the orientational order parameter (Figure 4b). TEM of the cross-linked mesophase aligned at low fields also revealed a dependence of alignment quality and grain size on field strength. For instance, the grain size of samples aligned at 2 T shown in Figures 4c and 4d was noticeably smaller than that of that observed for samples aligned at 6 T. The individual domains exhibited less continuity, and orientational defects were readily visible, such as the splay of column axes shown in Figure 4d. Accordingly, the Fourier transforms of the TEM images are much more diffuse than the sharp spots for the 6 T data shown in Figure 3.

The hydrophilic character of the ionic nanochannels of the Na-GA3C11 membranes makes these potentially useful materials for ion transport. Moreover the ionic conductivity of the membranes provides a useful measure of the degree of alignment of the system over macroscopic lateral dimensions. Mechanically robust membranes with a thickness of *ca.* 80 μm were prepared for ion conduction studies by either annealing the mesophase in the absence of the field or by rotation in a 6 T field to produce randomly or vertically aligned ionic nanochannels, respectively, in an electrode-sandwiched geometry. Information about the lateral and through-thickness uniformity of the alignment over more macroscopic dimensions than surveyed by TEM was provided by polarized optical microscopy characterization. Whereas the magnetic field-processed membrane exhibited optical extinction, indicating homeotropic alignment of the ionic nanochannels, the birefringent texture of the nonaligned membrane suggested random orientation of the ionic nanochannels (Figure 5a). The high transparency of the aligned film is consistent with the formation of an LC monodomain, whereas nonaligned films were invariably cloudy due to visible light scattering by the polydomain texture.

Both aligned and nonaligned materials were tough, mechanically coherent films, consistent with a high cross-link density, and illustrating the ability of the system to preserve the LC order during cross-linking (see photo in Figure 5b). The uniform orientation of the long axis of the ionic nanochannels along the film normal in the aligned membrane can be further confirmed by POM imaging of a small slice of the polymer film, where the normal of the membrane was positioned perpendicular to the direction of the light propagation as shown schematically in Figure 5c. By rotating the sample stage, the transmission intensity reached a minimum when the membrane normal was oriented either parallel or perpendicular to the

polarizer (0 or 90°), but it reached a maximum at an angle of 45°. This behavior provides strong evidence that the optic axis (*i.e.*, the long axis of the nanochannels) coincided with the membrane normal. The alignment is unambiguously confirmed by TEM investigations of the sandwiched films. The nanochannels are perpendicular to the film surface and can be clearly seen to persist all the way to the boundaries of the film (see Supporting Information Figures S9 and S10). This absence of a boundary layer with planar alignment induced by the confining surfaces of the sample is important as it eliminates boundary resistance to transport and the need for any postprocessing steps to remove any such layer in a working membrane.

Samples were allowed to equilibrate under 100% relative humidity at room temperature and then characterized for ionic conductivity by using AC impedance spectroscopy. Membranes with aligned nanochannels produced at 6 T show an 85-fold increase in their conductivity relative to nonaligned materials (Figure 5d). This result highlights the critical role that pore alignment plays in defining the transport properties and performance of nanoporous membranes.

Prior work has established the utility of soft mesophases in controlling the alignment and placement of anisotropic nanomaterials.[41−43] The ability of the wedge-shaped amphiphilic monomer Na-GA3C11 to align under magnetic fields and cross-link effectively suggests that this technique can serve as a platform to enable the scalable fabrication of functional nanocomposites in addition to nanoporous polymer membranes. We may envision, for example, the use of the aligned mesophase to control the assembly of anisotropic nanomaterials such as carbon nanotubes, metal nanowires or semiconducting nanorods within one domain to produce arrays of such nanomaterials vertically oriented in polymer films.

Toward this end, we also investigated the stability, alignment, and polymerization behavior of Na-GA3C11 in the presence of added water and an organic additive in the form of a lyotropic H_{II} mesophase, which may be used to facilitate the coassembly of nanomaterials of interest. We observed formation of a stable, homogeneous H_{II} lyotropic liquid crystal (LLC) phase by an appropriately composed mixture of Na-GA3C11, a polymerizable hydrophobic organic additive (butyl acrylate), and water as the lyotropic liquid phase. This H_{II} phase was capable of field alignment with excellent retention of its structure on polymerization, as confirmed by SAXS and TEM data (see Supporting Information Figure S11). This finding is compelling since functional nanomaterials as described above, or additives such as electrolytes and catalysts, can be incorporated into the cross-linkable LLC precursor phase to broaden the potential application spectrum of the resultant oriented, nanostructured polymer networks. Systematic studies on control over the alignment, polymerization, and functional properties (*i.e.*, water nanofiltration performance) of these aligned and cross-linked H_{II}-phase films will be addressed in a future report.

CONCLUSION

In conclusion, the facile fabrication of polymer membranes with large-area, vertically aligned, 1 nm channels has been demonstrated through magnetic field alignment and photo-cross-linking of the neat thermotropic Col_h and water-based lyotropic H_{II} mesophases formed by a wedge-shaped LC monomer. The system displays an impressive areal pore density of 2.5×10^{12} cm^{-2}. The scalability and high fidelity of this approach to forming vertically aligned, 1 nm ionic channels provide new opportunities in designing high performance polymer membranes for the selective removal of dissolved organic and ionic contaminants from feed streams, as well as the engineering of new types of functional nanocomposites with long-range order. The remarkable improvement in membrane ionic conductivity on alignment underlines the potential to optimize transport properties by appropriate control of microstructure.

EXPERIMENTAL SECTION

Materials. Na-GA3C11 was synthesized according to a previous report,[15] the details of which can be found in the Supporting Information. All chemicals were purchased from Aldrich and used as received. Neat Na-GA3C11 displays a thermotropic Col_h phase at room temperature and ambient pressure. The water-based lyotropic H_{II} phase of Na-GA3C11 in this study was formed by mixing Na-GA3C11 (88.5 wt %), butyl acrylate (8 wt %), and water (3 wt %, Milli-Q). This mixture was then mixed and equilibrated using methods described previously to form a H_{II} phase.[26,31] For UV-initiated radical cross-linking, diphenyl(2,4,6-trimethylbenzoyl)phosphine oxide (a commercially available radical photoinitiator) was mixed into the mesophases at a fixed weight percentage of 0.5 wt % of the total sample mass.

Differential Scanning Calorimetry (DSC). DSC measurements were performed using a Q200 DSC (TA Instruments) with a heating/cooling rate of 10 °C/min.

Polarizing Optical Microscopy (POM). POM studies were done by observation of samples using a Zeiss Axiovert 200 M inverted microscope.

X-ray Scattering. For *in situ* SAXS studies, a glass capillary with a 1.5 mm inner diameter was filled with the mesophase sample (without photoinitiator) and sealed by 5 min epoxy. The capillary was positioned in a rotary holder within the magnet. As schematically shown in Figure 2a, the X-ray beam, the magnetic field, and the rotation axis were orthogonal to each other. Temperature-resolved SAXS studies (0.1 °C/min) were performed using a customized Rigaku SMAX-3000 instrument with the accessible scattering vector (q) ranging from 0.015 to

0.21 $Å^{-1}$. The wavelength of the X-ray beam was 1.542 Å (Cu Kα radiation). 2-D SAXS patterns were recorded by a 2-D electronic wire detector and calibrated using a silver behenate standard (*d*-spacing of 58.38 Å). SAXS with higher *q* values as well as WAXS measurements on mesophases before and after cross-linking were performed using a Rigaku 007 HF+ instrument with a rotating anode Cu Kα X-ray source ($\lambda = 1.542$ Å) and a 2-D Saturn 994+ CCD detector. The calibrations of the resultant 2-D SAXS and WAXS patterns were done by using a silver behenate standard and a silicon powder standard (*d*-spacing of 3.1355 Å), respectively. All the 2-D scattering patterns were integrated into 1-D plots of scattering intensity (*I*) *versus q*, where $q = 4\pi \sin(\theta)/\lambda$ and the scattering angle is 2θ.

Transmission Electron Microscopy (TEM). Cross-linked samples were sectioned at room temperature by a diamond knife mounted on a Leica EM UC7 ultramicrotome. Thin sections with a thickness of about 60 nm were retrieved on TEM grids after flotation onto water and stained in vapor of a 0.5% aqueous solution of RuO_4 for 10 min. The benzene rings of the molecules were selectively stained. Sectioned samples were then visualized by FEI Tecnai Osiris TEM with an accelerating voltage of 200 kV.

Magnetic Field Alignment. Magnetic alignment was conducted using a superconducting magnet (American Magnetics, Inc.) with a field strength that can be varied from 0 to 6 T. Samples were rotated about an axis perpendicular to the magnetic field with a fixed speed of 4 rpm to achieve uniaxial alignment (except when a comparison was made with degenerate alignment in which samples were held statically). To magnetically align a mesophase, the sample was heated above the sample clearing point, followed by slow cooling back to room temperature. The temperature rate for all magnetic alignment experiments was fixed to 0.1 °C/min.

Preparation of Cross-linked Col_h and H_{II} Membranes. The Na-GA3C11 mesophase doped with radical photoinitiator (0.5 wt %) was sandwiched between two indium tin oxide (ITO)-coated glass substrates with an 80-μm-thick spacer. Vertical alignment of the ionic nanochannels was achieved by slowly cooling the mesophases at 0.1 °C/min from their isotropic states to room temperature in a 6 T magnetic field with simultaneous rotation of the substrate normal about an axis perpendicular to the field. For comparison, mesophases with random orientation was obtained by following the same annealing procedure while the magnetic field was quenched to 0 T. The aligned and nonaligned mesophases were photo-cross-linked immediately by exposure to 365 nm UV light (8W UVL-18 EL lamp at a distance of *ca*. 10 cm) for 24 h at room temperature, resulting in a mechanically robust polymer film of a circular shape with diameter of approximately 1.6 cm.

Ionic Conductivity Measurements. The membrane sample was sandwiched between ITO-coated electrodes and then connected to the two terminals of a Solartron 1260 Frequency Response Analyzer *via* the ITO electrodes. The AC voltage amplitude was varied from 10 to 150 mV to ensure that the system response in the range tested was linear, and a 100 mV voltage amplitude was chosen for all the measurements. The samples were then placed in a humidity box, and the relative humidity of the chamber was varied from 60 to 100% using a homemade humidity chamber. The AC voltage frequency was swept in between 50 mHz to 1 MHz. Each sample was let to equilibrate for 12 h at room temperature before the measurement was performed. AC impedance spectroscopy was performed at room temperature, and the through-plane conductance was estimated by fitting the frequency response of the system to an appropriate equivalent circuit.[44] A Nyquist plot of the EIS measurement used to estimate the ionic conductivity of cross-linked aligned and nonaligned films at a relative humidity of 100% can be found in the Supporting Information (Figure S12). After conductivity measurement the film was removed, and the film thickness and geometric surface area were measured to determine the ionic conductivity of the materials.

Conflict of Interest: The authors declare no competing financial interest.

Supporting Information Available: Large-area TEM images, DSC of mesophases and synthetic procedures are detailed. This material is available free of charge *via* the Internet at http://pubs.acs.org.

Acknowledgment. The work performed at Yale was supported by NSF (CMMI-1246804). The authors thank Mike Degen (Rigaku, Inc.), Brandon Mercado (Yale CBIC), and AMI Inc. for technical support. C.O.O. acknowledges additional financial support from NSF (DMR-0847534; DMR-1119826) and from a 3M Nontenured Faculty Award. M.E.T. acknowledges support from the NSG Graduate Research Fellowship DGE-1122492. Facilities use at Yale was supported by the YINQE and NSF MRSEC program (DMR-1119826). M.G.C., B.R.W., R.D.N., and D.L.G. acknowledge the DOE APRA-e program (D1-AR0000098) and the U.S. Bureau of Reclamation (R13AC80040) for partial support of the monomer synthesis work done at CU Boulder.

REFERENCES AND NOTES

1. Yoon, J.; Lee, W.; Thomas, E. L. Self-Assembly of Block Copolymers for Photonic-Bandgap Materials. *MRS Bull.* **2005**, *30*, 721–726.
2. Jackson, E. A.; Hillmyer, M. A. Nanoporous Membranes Derived from Block Copolymers: From Drug Delivery to Water Filtration. *ACS Nano* **2010**, *4*, 3548–3553.
3. Majewski, P. W.; Gopinadhan, M.; Osuji, C. O. Understanding Anisotropic Transport in Self-Assembled Membranes and Maximizing Ionic Conductivity by Microstructure Alignment. *Soft Matter* **2013**, *9*, 7106–7116.
4. Gin, D. L.; Noble, R. D. Designing the Next Generation of Chemical Separation Membranes. *Science* **2011**, *332*, 674–676.
5. Merkel, T. C.; Freeman, B. D.; Spontak, R. J.; He, Z.; Pinnau, I.; Meakin, P.; Hill, A. J. Ultrapermeable, Reverse-Selective Nanocomposite Membranes. *Science* **2002**, *296*, 519–522.
6. Dorin, R. M.; Phillip, W. A.; Sai, H.; Werner, J.; Elimelech, M.; Wiesner, U. Designing Block Copolymer Architectures for Targeted Membrane Performance. *Polymer* **2014**, *55*, 347–353.
7. Elabd, Y. A.; Hickner, M. A. Block Copolymers for Fuel Cells. *Macromolecules* **2010**, *44*, 1–11.
8. Young, W.-S.; Kuan, W.-F.; Epps, T. H. Block Copolymer Electrolytes for Rechargeable Lithium Batteries. *J. Polym. Sci., Part B: Polym. Phys.* **2014**, *52*, 1–16.
9. Cushen, J. D.; Otsuka, I.; Bates, C. M.; Halila, S.; Fort, S.; Rochas, C.; Easley, J. A.; Rausch, E. L.; Thio, A.; Borsali, R.; Willson, C. G.; Ellison, C. J. Oligosaccharide/Silicon-Containing Block Copolymers with 5 nm Features for Lithographic Applications. *ACS Nano* **2012**, *6*, 3424–3433.
10. Kennemur, J. G.; Yao, L.; Bates, F. S.; Hillmyer, M. A. Sub-5 nm Domains in Ordered Poly(cyclohexylethylene)-block-poly(methyl methacrylate) Block Polymers for Lithography. *Macromolecules* **2014**, *47*, 1411–1418.
11. Shannon, M. A.; Bohn, P. W.; Elimelech, M.; Georgiadis, J. G.; Marinas, B. J.; Mayes, A. M. Science and Technology for Water Purification in the Coming Decades. *Nature* **2008**, *452*, 301–310.
12. Broer, D. J.; Bastiaansen, C. M. W.; Debije, M. G.; Schenning, A. P. H. J. Functional Organic Materials Based on Polymerized Liquid-Crystal Monomers: Supramolecular Hydrogen-Bonded Systems. *Angew. Chem., Int. Ed.* **2012**, *51*, 7102–7109.
13. Zhou, M.; Nemade, P. R.; Lu, X.; Zeng, X.; Hatakeyama, E. S.; Noble, R. D.; Gin, D. L. New Type of Membrane Material for Water Desalination Based on a Cross-Linked Bicontinuous Cubic Lyotropic Liquid Crystal Assembly. *J. Am. Chem. Soc.* **2007**, *129*, 9574–9575.
14. Beginn, U.; Zipp, G.; Möller, M. Functional Membranes Containing Ion-Selective Matrix-Fixed Supramolecular Channels. *Adv. Mater.* **2000**, *12*, 510–513.
15. Lee, H.-K.; Lee, H.; Ko, Y. H.; Chang, Y. J.; Oh, N.-K.; Zin, W.-C.; Kim, K. Synthesis of a Nanoporous Polymer with Hexagonal Channels from Supramolecular Discotic Liquid Crystals. *Angew. Chem., Int. Ed.* **2001**, *40*, 2669–2671.
16. Sorenson, G. P.; Coppage, K. L.; Mahanthappa, M. K. Unusually Stable Aqueous Lyotropic Gyroid Phases from

Gemini Dicarboxylate Surfactants. *J. Am. Chem. Soc.* **2011**, *133*, 14928–14931.
17. Gin, D. L.; Lu, X.; Nemade, P. R.; Pecinovsky, C. S.; Xu, Y.; Zhou, M. Recent Advances in the Design of Polymerizable Lyotropic Liquid-Crystal Assemblies for Heterogeneous Catalysis and Selective Separations. *Adv. Funct. Mater.* **2006**, *16*, 865–878.
18. van Kuringen, H. P.; Eikelboom, G. M.; Shishmanova, I. K.; Broer, D. J.; Schenning, A. P. Responsive Nanoporous Smectic Liquid Crystal Polymer Networks as Efficient and Selective Adsorbents. *Adv. Funct. Mater.* **2014**, *24*, 5045–5051.
19. Soberats, B.; Uchida, E.; Yoshio, M.; Kagimoto, J.; Ohno, H.; Kato, T. Macroscopic Photocontrol of Ion-Transporting Pathways of a Nanostructured Imidazolium-Based Photoresponsive Liquid Crystal. *J. Am. Chem. Soc.* **2014**, *136*, 9552–9555.
20. Yoshio, M.; Kagata, T.; Hoshino, K.; Mukai, T.; Ohno, H.; Kato, T. One-Dimensional Ion-Conductive Polymer Films: Alignment and Fixation of Ionic Channels Formed by Self-Organization of Polymerizable Columnar Liquid Crystals. *J. Am. Chem. Soc.* **2006**, *128*, 5570–5577.
21. Shimura, H.; Yoshio, M.; Hamasaki, A.; Mukai, T.; Ohno, H.; Kato, T. Electric-Field-Responsive Lithium-Ion Conductors of Propylenecarbonate-Based Columnar Liquid Crystals. *Adv. Mater.* **2009**, *21*, 1591–1594.
22. Forney, B. S.; Baguenard, C.; Guymon, C. A. Effects of Controlling Polymer Nanostructure Using Photopolymerization within Lyotropic Liquid Crystalline Templates. *Chem. Mater.* **2013**, *25*, 2950–2960.
23. Hu, H.; Gopinadhan, M.; Osuji, C. O. Directed Self-Assembly of Block Copolymers: A Tutorial Review of Strategies for Enabling Nanotechnology with Soft Matter. *Soft Matter* **2014**, *10*, 3867–3889.
24. Zhang, H.; Li, L.; Möller, M.; Zhu, X.; Rueda, J. J. H.; Rosenthal, M.; Ivanov, D. A. From Channel-Forming Ionic Liquid Crystals Exhibiting Humidity-Induced Phase Transitions to Nanostructured Ion-Conducting Polymer Membranes. *Adv. Mater.* **2013**, *25*, 3543–3548.
25. Chen, Y.; Lingwood, M. D.; Goswami, M.; Kidd, B. E.; Hernandez, J. J.; Rosenthal, M.; Ivanov, D. A.; Perlich, J.; Zhang, H.; Zhu, X.; Möller, M.; Madsen, L. A. Humidity-Modulated Phase Control and Nanoscopic Transport in Supramolecular Assemblies. *J. Phys. Chem. B* **2014**, *118*, 3207–3217.
26. Smith, R. C.; Fischer, W. M.; Gin, D. L. Ordered Poly(p-phenylenevinylene) Matrix Nanocomposites *via* Lyotropic Liquid-Crystalline Monomers. *J. Am. Chem. Soc.* **1997**, *119*, 4092–4093.
27. Deng, H.; Gin, D. L.; Smith, R. C. Polymerizable Lyotropic Liquid Crystals Containing Transition-Metal and Lanthanide Ions: Architectural Control and Introduction of New Properties into Nanostructured Polymers. *J. Am. Chem. Soc.* **1998**, *120*, 3522–3523.
28. Zhu, X.; Scherbina, M. A.; Bakirov, A. V.; Gorzolnik, B.; Chvalun, S. N.; Beginn, U.; Möller, M. Methacrylated Self-Organizing 2,3,4-Tris(alkoxy)benzenesulfonate: A New Concept toward Ion-Selective Membranes. *Chem. Mater.* **2006**, *18*, 4667–4673.
29. Resel, R.; Theissl, U.; Gadermaier, C.; Zojer, E.; Kriechbaum, M.; Amenitsch, H.; Gin, D.; Smith, R.; Leising, G. The H2-Phase of the Lyotropic Liquid Crystal Sodium 3,4,5-Tris(omega-acryloyloxyundecyloxy)benzoate. *Liq. Cryst.* **2000**, *27*, 407–411.
30. Resel, R.; Leising, G.; Markart, P.; Kriechbaum, M.; Smith, R.; Gin, D. Structural Properties of Polymerised Lyotropic Liquid Crystals Phases of 3,4,5-Tris(ω-acryloxyalkoxy)-benzoate Salts. *Macromol. Chem. Phys.* **2000**, *201*, 1128–1133.
31. Zhou, M.; Kidd, T. J.; Noble, R. D.; Gin, D. L. Supported Lyotropic Liquid-Crystal Polymer Membranes: Promising Materials for Molecular-Size-Selective Aqueous Nanofiltration. *Adv. Mater.* **2005**, *17*, 1850–1853.
32. Firouzi, A.; Schaefer, D. J.; Tolbert, S. H.; Stucky, G. D.; Chmelka, B. F. Magnetic-Field-Induced Orientational Ordering of Alkaline Lyotropic Silicate–Surfactant Liquid Crystals. *J. Am. Chem. Soc.* **1997**, *119*, 9466–9477.
33. de Gennes, P. G.; Prost, J. *The Physics of Liquid Crystals*; Clarendon Press: Oxford, U.K., 1995.
34. Burnell, E.; de Lange, C. A. *NMR of Ordered Liquids*; Springer: Berlin, 2003.
35. Majewski, P. W.; Osuji, C. O. Non-degenerate Magnetic Alignment of Self-Assembled Mesophases. *Soft Matter* **2009**, *5*, 3417–3421.
36. Lee, J.-H.; Choi, S.-M.; Pate, B. D.; Chisholm, M. H.; Han, Y.-S. Magnetic Uniaxial Alignment of the Columnar Superstructure of Discotic Metallomesogens over the Centimetre Length Scale. *J. Mater. Chem.* **2006**, *16*, 2785–2791.
37. Majewski, P. W.; Osuji, C. O. Controlled Alignment of Lamellar Lyotropic Mesophases by Rotation in a Magnetic Field. *Langmuir* **2010**, *26*, 8737–8742.
38. Percec, V.; Imam, M. R.; Peterca, M.; Wilson, D. A.; Graf, R.; Spiess, H. W.; Balagurusamy, V. S. K.; Heiney, P. A. Self-Assembly of Dendronized Triphenylenes into Helical Pyramidal Columns and Chiral Spheres. *J. Am. Chem. Soc.* **2009**, *131*, 7662–7677.
39. Gearba, R. I.; Anokhin, D. V.; Bondar, A. I.; Bras, W.; Jahr, M.; Lehmann, M.; Ivanov, D. A. Homeotropic Alignment of Columnar Liquid Crystals in Open Films by Means of Surface Nanopatterning. *Adv. Mater.* **2007**, *19*, 815–820.
40. Tran, H.; Gopinadhan, M.; Majewski, P. W.; Shade, R.; Steffes, V.; Osuji, C. O.; Campos, L. M. Monoliths of Semiconducting Block Copolymers by Magnetic Alignment. *ACS Nano* **2013**, *7*, 5514–5521.
41. Kao, J.; Thorkelsson, K.; Bai, P.; Zhang, Z.; Sun, C.; Xu, T. Rapid Fabrication of Hierarchically Structured Supramolecular Nanocomposite Thin Films in One Minute. *Nat. Commun.* **2014**, *5*, 4053.
42. Liu, Q.; Cui, Y.; Gardner, D.; Li, X.; He, S.; Smalyukh, I. I. Self-Alignment of Plasmonic Gold Nanorods in Reconfigurable Anisotropic Fluids for Tunable Bulk Metamaterial Applications. *Nano Lett.* **2010**, *10*, 1347–1353.
43. Mauter, M. S.; Elimelech, M.; Osuji, C. O. Nanocomposites of Vertically Aligned Single-Walled Carbon Nanotubes by Magnetic Alignment and Polymerization of a Lyotropic Precursor. *ACS Nano* **2010**, *4*, 6651–6658.
44. Soboleva, T.; Xie, Z.; Shi, Z.; Tsang, E.; Navessin, T.; Holdcroft, S. Investigation of the through-Plane Impedance Technique for Evaluation of Anisotropy of Proton Conducting Polymer Membranes. *J. Electroanal. Chem.* **2008**, *622*, 145–152.